Letter

Multipolar nematic state of nonmagnetic FeSe based on DFT+U

Takemi Yamada [*] and Takami Tohyama

Department of Applied Physics, Facility of Science, Tokyo University of Science, 6-3-1 Niijuku, Katsushika, Tokyo 125-8585, Japan

(Received 15 July 2021; revised 5 September 2021; accepted 28 September 2021; published 12 October 2021)

Clarifying the origin of nematic state in FeSe is one of urgent problems in the field of iron-based superconductivity. Motivated by the discovery of a nematic solution in the density-functional theory implemented by on-site Coulomb interaction (DFT+U) [npj Quantum Mater. **5**, 50 (2020)], we reexamine the U dependence of electronic states in the nonmagnetic normal state of FeSe and perform full multipolar analyses for the nematic state. We find that with increasing U the normal state experiences a topological change in the Fermi surfaces before the emergence of a nematic ground state. The resulting nematic ground state is a multipolar state having both antiferrohexadecapoles in the E representation and ferromultipoles in the B_2 representation on each Fe site. Cooperative coupling between the E and the B_2 multipoles in the local coordinate with the D_{2d} point group will play an important role in the formation of the d_{xz}, d_{yz} orbital-splitting nematic state not only in FeSe, but also in other iron pnictides.

DOI: 10.1103/PhysRevB.104.L161110

FeSe [1,2] is one of the most intensively studied iron-based superconductors [3–7] because of its complex and versatile ground state under pressure P [8–10] and substitution of Se [11,12]. Below the tetragonal-orthorhombic structural phase transition at $T_S = 90$ K, the electronic state of FeSe shows a behavior of the nematic state breaking the C_4 rotational symmetry whereas keeping translational symmetry without any magnetic ordering unlike other iron-based superconductors. Despite a tiny orthorhombicity [13], the system exhibits a large band splitting associated with the orbital differentiation of d_{xz}, d_{yz}, $|E_{yz} - E_{xz}| = 50$ meV [14], which is too large to attribute to the lattice deformation. This strongly supports the electronic origin of the nematic state, being consistent with the enhancement of the nematic fluctuation when T approaches T_S as observed in the nematic susceptibility [11,15] and the electronic Raman response [16,17]. Therefore, the clarification of the nematic state is significant for the microscopic understanding of recent interesting phenomena, such as the orbital-selective correlation effect [18–21] and the BCS-BEC crossover [22–25].

The Fermi surface (FS) and low-energy band structures of FeSe have extensively been investigated [14,26–38] where the multiorbital compensated metal with Fe-d orbitals is confirmed [6,7]. In the normal (nonnematic) state, two hole FSs (2h-FSs) around Γ and two-electron FSs (2e-FSs) around M have commonly been reported, but their size is extremely small only occupied 2-3% in the Brillouin zone (BZ). These small FSs and the low-energy band structure have not still been reproduced by the density-functional theory (DFT) [37], DFT+U [38], the dynamical mean-field theory (DMFT) [18–20,39], and the quasiparticle self-consistent GW [40]. Several studies based on adjusted models to reproduce the low-energy bands of angle-resolved photoemission spectroscopy (ARPES) [31] can explain the enhancement of orbital and magnetic fluctuations in the T-P phase [41–43].

As for the nematic state, several FSs have been reported by the Shubnikov–de Haas [26,27] and ARPES experiments [14,28–36] where a single hole FS (1h-FS) near Γ is common whereas it is still unsettled whether the electron FS near M is a single (1e-FS) or two. The sign change in the orbital splitting at Γ and M points in the BZ has been observed [30,31], whose origin and mechanism have been discussed [44–47]. The recent DFT study [48] has provided a new nematic ground state with the E_u irreducible representation of the D_{4h} symmetry, which contains 1e-FS and additional hybridization between d_{xy} and d_{xz}, d_{yz} orbitals [49,50]. Although this nematic state seems to explain the recent experiment [36], it is unclear how the nematic state is reached from the well-known three-hole FSs (3h-FSs) of the DFT normal state [38,48]. Therefore, a systematic investigation of the normal state on the verge of nematic ordering and a detailed multipolar analysis in the nematic state are highly desirable.

In this Letter, we examine the U dependence of the electronic states of FeSe by the DFT+U method and find a topological change in FSs before a nematic order occurs. The resulting nematic ground state is found to be a multipolar state having both antiferrohexadecapoles in the E representation and ferromultipoles in the B_2 representation on each Fe site with the locally D_{2d} point group. This coexistence indicates that cooperative coupling between the E and the B_2 multipoles can be a source of the formation of the d_{xz}, d_{yz} orbital-splitting nematic state in FeSe and related materials.

We have performed the DFT+U calculation [51] in the first-principles code WIEN2K [52] where the Coulomb interaction U for d electrons in the muffin-tin (MT) radius $R^{\nu}_{\rm MT}$ with atomic sites $\nu = $ Fe1, Fe2 in the unit cell is introduced. The DFT+U correction energy consists of total occupation number of d electrons within $R^{\nu}_{\rm MT}$, $n^{d,\nu} = \sum_{m\sigma} n^{\sigma,\nu}_{mm}$, and the

[*] t-yamada@rs.tus.ac.jp

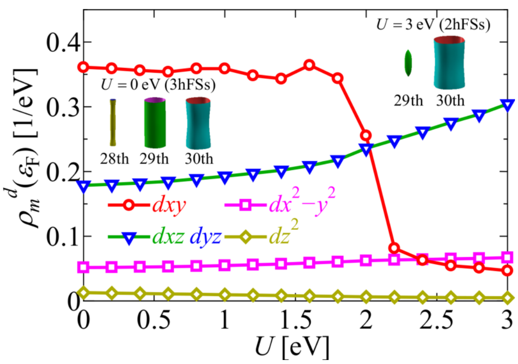

FIG. 1. U dependence of pDOS $\rho_m^d(\varepsilon_F)$. The inset shows the 3h-FSs for $U = 0$ eV (left center) and the 2h-FSs for $U = 3$ eV (right top).

density-matrix $n_{mm'}^{\sigma,\nu}$ as explicitly shown in Ref. [51]. Hereafter we drop the spin index σ and use $n_{mm'}^{\uparrow,\nu} = n_{mm'}^{\downarrow,\nu} = n_{mm'}^{\nu}$ and $n_{mm}^{\nu} = n_m^{\nu}/2$ due to the nonmagnetic situation throughout the paper [51]. By solving the Kohn-Sham equation self-consistently, the band energy $\varepsilon_{\boldsymbol{k}n}$ with wave-vector $\boldsymbol{k}$ and band-index n is obtained for any given U where the effective $+U$ potential acting on the atomic basis $v_{mm'}^{\nu}$ [53,54] is given by

$$v_{mm'}^{\nu} = \delta_{mm'}\frac{U}{2}\left(1 - n_m^{\nu}\right) + (1 - \delta_{mm'})\left(-U n_{mm'}^{\nu}\right), \qquad (1)$$

where the first (second) term in Eq. (1) is proportional to the diagonal (off-diagonal) density-matrix n_{mm}^{ν} ($n_{mm'}^{\nu}$). All the technical details are presented in Ref. [51].

First, we investigate the U dependence of the normal electronic state in FeSe. Figure 1 shows the partial density-of-states (pDOS) $\rho_m^d(\varepsilon_F)$ at the Fermi energy ε_F. When $U = 0$ eV, 3h-FSs consisting of the 28th, 29th, and 30th bands are obtained as shown in the inset of Fig. 1, being similar to the previous DFT results [37,38]. With increasing U, $\rho_m^d(\varepsilon_F)$ of d_{xy} orbital drops at $U \simeq 2$ eV ($=U_{\rm LT}$), whereas, in turn, that of d_{xz}, d_{yz} increases gradually. Since the 28th band constructing the most inner hole FS originates from the d_{xy} orbital, it falls below ε_F and the FS vanishes at a Lifshitz transition point $U_{\rm LT}$ where the 3h-FSs change to the 2h-FSs from the 29th and 30th bands as shown in the inset of Fig. 1 [55]. This change is caused by $v_U(\boldsymbol{r})$ that induces orbital-dependent energy shifts, being proportional to $1 - n_m^{\nu}$ as shown in the first term of Eq. (1). We can find that the occupied number n_m^d in d_{xy} and d_{z^2} at $U = 0$ eV, which is larger than in d_{xz}, d_{yz}, and $d_{x^2-y^2}$, increases further with increasing U, resulting in the negatively large value of $1 - n_m^{\nu}$ in d_{xy} [56].

In contrast to the h-FSs, the e-FSs from the 31st and 32nd bands with d_{xz}, d_{yz} orbitals at M and A points do not undergo any topological change but, instead, $\varepsilon_{\boldsymbol{k}n}$ of these bands approaches ε_F monotonically with increasing U. This manifestation of the d_{xz}, d_{yz} orbitals near ε_F as evidenced by the 2h-FSs and e-FSs will triggers the formation of a nematic state mentioned below.

Next we calculate a nematic solution by preconditioning the initial charge density [51] as was performed in the previous pseudopotential calculation [48]. Figure 2(a) shows the total energy difference between the normal and the nematic

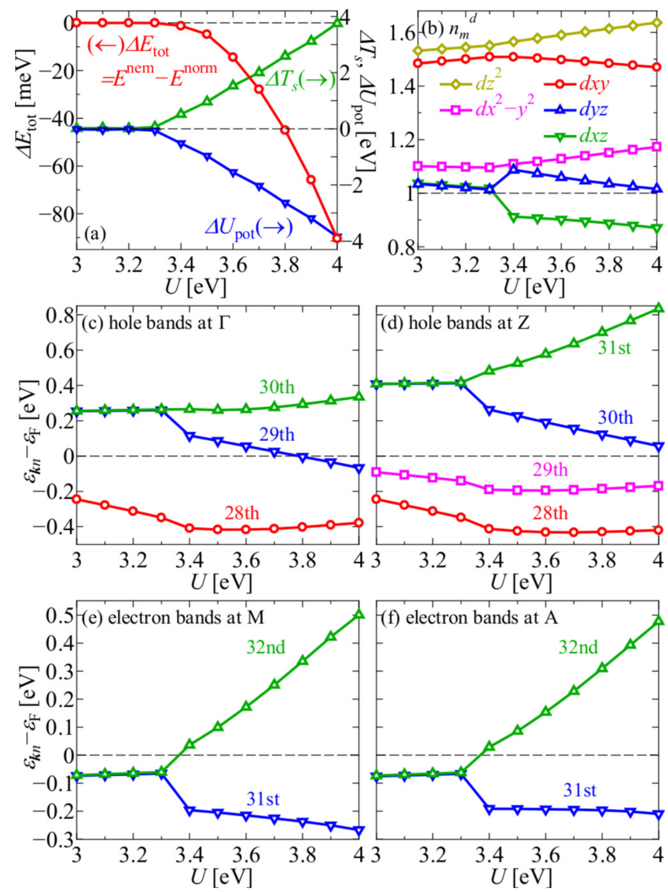

FIG. 2. (a) Energy differences of the total energy $\Delta E_{\rm tot}$ (left axis), and kinetic and potential energies ΔT_s, $\Delta U_{\rm pot}$ (right axis) and (b) n_m^d. (c)–(f) The obtained band energy $\varepsilon_{\boldsymbol{k}n} - \varepsilon_F$ around ε_F for $U = 3$ to 4 eV.

states $\Delta E_{\rm tot} = E_{\rm tot}^{\rm nem} - E_{\rm tot}^{\rm normal}$ as a function of U together with the kinetic-energy and potential-energy differences ΔT_s and $\Delta U_{\rm pot}$, where $E_{\rm tot} = T_s + U_{\rm pot}$ is calculated by the total energy formula of the all-electron method [57] under the Virial theorem $2T_s + U_{\rm pot} = 0$. With increasing U more than $U = 3.4$ eV, $\Delta E_{\rm tot} < 0$ is realized with $\Delta T_s > 0$ and $\Delta U_{\rm pot} < 0$ together with the occupied number splitting between d_{xz} and d_{yz} orbitals as shown in Fig. 2(b). The energy gain is on the order of $O(10^{1\text{-}2}$ meV), which basically agrees with the previous pseudopotential DFT result [48].

The U dependence of $\varepsilon_{\boldsymbol{k}n} - \varepsilon_F$ near ε_F at Γ and Z [M and A] points are shown in Figs. 2(c) and 2(d) [Figs. 2(e) and 2(f)], respectively. The d_{xz}- and d_{yz}-orbital bands, whose number is denoted in the figures, split due to the nematic state transition. Since the 32nd band in M and A points rises above ε_F, 2e-FSs in the nonnematic state change to 1e-FS in the nematic state. Combining with the change from 2h-FSs to 1h-FS at Γ point above $U = 3.7$ eV, we find the number of FSs consistent with the experiment [36] and the previous DFT result [48].

The order parameters of the nematic state obtained by DFT+U have been discussed in a previous study [48] where only finite off-diagonal density-matrix elements are taken into account. Here, we derive all the active multipole moments

TABLE I. The definition and notations of multipole X_α denoted by quadrupole O_{Γ_γ} and hexadecapole $Q_{4\Gamma_\gamma}$ together with the irreducible representations (IRRs) in D_{2d} symmetry [58,59] at each Fe site. $T_{kq}^{(c,s)}$ (T_{kq}) is the tesseral (spherical) tensor operator with a relation $T_{kq}^{(c,s)} = \frac{(-1)^q}{\sqrt{2}}(T_{kq}^\dagger \pm T_{kq})$.

IRR	X_α	Tesseral tensor representation	(x, y, z) representation
A_1	O_u	T_{20}	$\frac{1}{2}(3z^2-r^2)$
	Q_4	$\sqrt{\frac{5}{12}}T_{44}^{(c)} + \sqrt{\frac{7}{12}}T_{40}$	$\frac{5\sqrt{21}(x^4+y^4+z^4-\frac{3}{5}r^4)}{12}$
	Q_{4u}	$-\sqrt{\frac{7}{12}}T_{44}^{(c)} + \sqrt{\frac{5}{12}}T_{40}$	$\frac{7\sqrt{15}[2z^4-x^4-y^4-\frac{6}{7}r^2(3z^2-r^2)]}{12}$
A_2	$Q_{4\alpha,z}$	$-T_{44}^{(s)}$	$\frac{\sqrt{35}}{2}xy(x^2-y^2)$
B_1	O_v	$T_{22}^{(c)}$	$\frac{\sqrt{3}}{2}(x^2-y^2)$
	Q_{4v}	$-T_{42}^{(c)}$	$\frac{7\sqrt{5}[x^4-y^4-\frac{6}{7}r^2(x^2-y^2)]}{4}$
B_2	O_{xy}	$T_{22}^{(s)}$	$\sqrt{3}xy$
	$Q_{4\beta,z}$	$T_{42}^{(s)}$	$\frac{\sqrt{5}}{2}xy(7z^2-r^2)$
E	O_{zx}, O_{yz}	$T_{21}^{(c)}, T_{21}^{(s)}$	$\sqrt{3}zx, \sqrt{3}yz$
	$Q_{4\alpha,x}$	$-\sqrt{\frac{1}{8}}T_{43}^{(s)} - \sqrt{\frac{7}{8}}T_{41}^{(s)}$	$\frac{\sqrt{35}}{2}yz(y^2-z^2)$
	$Q_{4\alpha,y}$	$-\sqrt{\frac{1}{8}}T_{43}^{(c)} + \sqrt{\frac{7}{8}}T_{41}^{(c)}$	$\frac{\sqrt{35}}{2}zx(z^2-x^2)$
	$Q_{4\beta,x}$	$\sqrt{\frac{7}{8}}T_{43}^{(s)} - \sqrt{\frac{1}{8}}T_{41}^{(s)}$	$\frac{\sqrt{5}}{2}yz(7x^2-r^2)$
	$Q_{4\beta,y}$	$-\sqrt{\frac{7}{8}}T_{43}^{(c)} - \sqrt{\frac{1}{8}}T_{41}^{(c)}$	$\frac{\sqrt{5}}{2}zx(7y^2-r^2)$

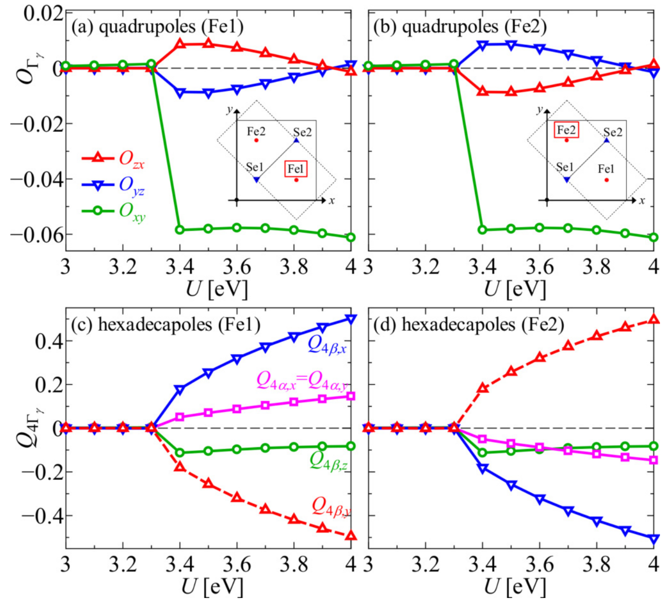

FIG. 3. The quadrupole and hexadecapole moments (a) and (b) O_{Γ_γ} and (c) and (d) $Q_{4\Gamma_\gamma}$ on Fe1 [(a) and (c)] and Fe2 [(b) and (d)] sites as a function of U. In the insets of (a) and (b), atom sites in the unit cell are depicted with x, y axes.

in the present system more generally [58,59]. Without the spin-orbit interaction, the multipole operator can be regarded as a power series expansion of the rank k of orbital angular momentum operator $\boldsymbol{\ell} = (\ell_x, \ell_y, \ell_z)$. Only the even rank multipoles, i.e., quadrupoles ($k = 2$) and hexadecapoles ($k = 4$), become finite for the d electron basis in each Fe site due to the time-reversal symmetry. These multipoles are classified by the irreducible representations $\{A_1, A_2, B_1, B_2, E\}$ at the Fe site with D_{2d} symmetry, which are summarized in Table I.

We calculate all the multipole moments listed in Table I from the density-matrix $n_{mm'}^{\nu}$ where all the multipole operators are normalized as $\mathrm{Tr}[X_\alpha X_\beta] = \delta_{\alpha\beta}$. We note that a similar approach has been performed on the magnetic multipole order in the actinide dioxides [60,61]. We find that the multipoles directly related to the nematic order are those in the B_2 and E representations. Figures 3(a) and 3(c) [3(b) and 3(d)] show the U dependence of the quadrupoles O_{xz}, O_{yz}, O_{xy}, and the hexadecapoles $Q_{4\beta,z}$, $Q_{4\alpha,x}$, $Q_{4\alpha,y}$, $Q_{4\beta,x}$, $Q_{4\beta,y}$ at the Fe1 [Fe2] site, respectively. Above $U = 3.4$ eV, the B_2 quadrupole moment for O_{xy} at the two Fe sites becomes negative as seen in Figs. 3(a) and 3(b) and the similar behavior is obtained for the B_2 hexadecapole $Q_{4\beta,z}$ as seen in Figs. 3(c) and 3(d). This behavior corresponds to the emergence of a ferronematic order associated with the orbital differentiation between d_{xz} and d_{yz}. On the other hand, the E hexadecapole moments for $Q_{4\alpha,x}$, $Q_{4\alpha,y}$, $Q_{4\beta,x}$, and $Q_{4\beta,y}$ are more than ten times larger than the E quadrupole moments for O_{xz}, O_{yz}. It is also interesting to note that $Q_{4\beta,x} > 0$, $Q_{4\beta,y} < 0$, and $Q_{4\alpha,x(y)} > 0$ at Fe1 but opposite signs at Fe2 as shown in Figs. 3(c) and 3(d). Namely, the E-type order parameter at Fe1 (Fe2) is written as $\pm(aQ_{4\alpha}^E + bQ_{4\beta}^E + cO^E)$, where $Q_{4\alpha(\beta)}^E = \frac{1}{\sqrt{2}}(Q_{4\alpha(\beta),x} \pm Q_{4\alpha(\beta),y})$ and $O^E = \frac{1}{\sqrt{2}}(O_{zx} - O_{yz})$ with $a^2 + b^2 + c^2 = 1$. This result indicates that the antiferro-ordering of the E multipoles with opposite values at two Fe sites coexists with the ferro-ordering of the B_2 multipoles with the same values at two sites.

Such the coexistence of E- and B_2-type multipoles can be understood from the phenomenological intermultipole coupling theory [58,62] at finite temperature T, where the Ginzburg-Landau free energy with the mean-field (MF) approximation can be expanded by the multipole moment X_α around the nematic transition as given by $F_{\mathrm{MF}} = F_{\mathrm{MF}}^{(2\mathrm{nd})} + F_{\mathrm{MF}}^{(3\mathrm{rd})} + \cdots$. Here, $F_{\mathrm{MF}}^{(3\mathrm{rd})} = -\frac{T}{3!}\sum_{\alpha\beta\gamma} g_{\alpha\beta\gamma}X_\alpha X_\beta X_\gamma$, where $X_\alpha = O_{\Gamma_\gamma}$ or $Q_{4\Gamma_\gamma}$ and $g_{\alpha\beta\gamma}$ is the symmetric constant defined as $g_{\alpha\beta\gamma} = \frac{1}{2d}\mathrm{Tr}[(X_\alpha X_\beta + X_\beta X_\alpha)X_\gamma]$ [63] with matrix dimension $d = 5$. The coupling terms among O_{xy}, $Q_{4\beta,z}$, and E multipoles are explicitly given by $F_{\mathrm{MF}}^{(3\mathrm{rd})} = -Tc_1 O_{xy}(-\frac{4}{11}O_{xz}O_{yz} - \frac{7}{11}Q_{4\alpha,x}Q_{4\alpha,y} + Q_{4\beta,x}Q_{4\beta,y}) - Tc_2 Q_{4\beta,z}(O_{xz}O_{yz} - \frac{7}{8}Q_{4\alpha,x}Q_{4\alpha,y} + Q_{4\beta,x}Q_{4\beta,y})$, where $c_1(c_2) = \frac{11}{84}\sqrt{\frac{15}{14}}(\frac{1}{21}\sqrt{\frac{10}{7}})$ and the second and third terms in both parentheses correspond to the coupling between the E multipoles and are negative whereas the coefficients of both parentheses including the B_2 multipoles are positive as shown in Fig. 3. Therefore, $F_{\mathrm{MF}}^{(3\mathrm{rd})}$ becomes negative as a whole stabilizing the coexistence state.

Finally, we discuss the band structure and orbital components of the normal ($U = 3.3$ eV) and nematic ($U = 3.4$ eV) states as shown in Figs. 4(a)–4(c) and 4(d)–4(f), respectively. It is clearly observed that the degenerated d_{xz} and d_{yz} bands near 0.25 eV (0.5 eV) at the Γ (Z) point split in the nematic state, corresponding to the ordering of O_{xy} and $Q_{4\beta,z}$ as seen in Fig. 3. Band splitting due to the same mechanism is also realized in the 31st and 32nd electron bands near 0 eV along the M-A direction, which consist of linear combinations of d_{xz} and d_{yz} orbitals without k_z dependence. This

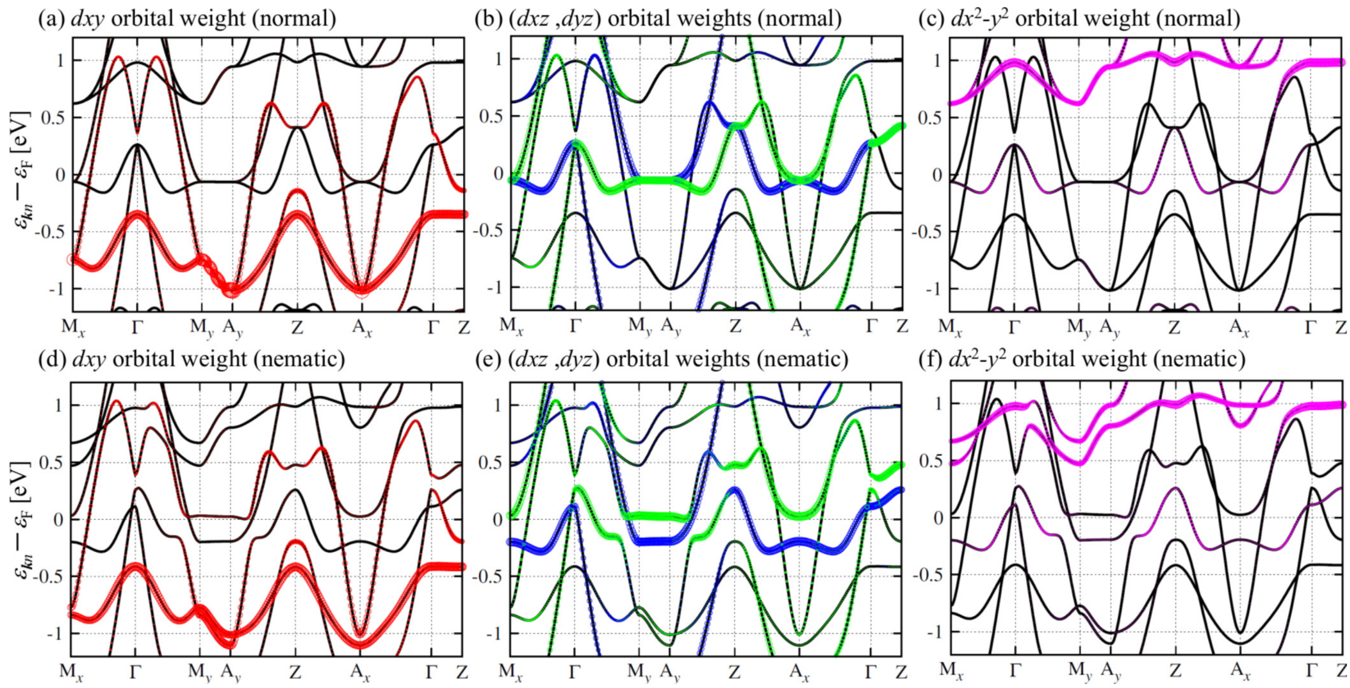

FIG. 4. Band structures for (a)–(c) normal state ($U = 3.3$ eV) and (d)–(f) nematic state ($U = 3.4$ eV) with the orbital weight of (a) and (d) d_{xy}, (b) and (e) d_{xz}(green), d_{yz} (blue), and (c) and (f) $d_{x^2-y^2}$ along the high-symmetry line in the BZ, where $\mathrm{M}_x[\mathrm{M}_y] = (\frac{\pi}{a}, \frac{\pi}{a}, 0)][(\frac{\pi}{a}, -\frac{\pi}{a}, 0)]$ and $A_x[A_y] = (\frac{\pi}{a}, \frac{\pi}{a}, \frac{\pi}{c})[(\frac{\pi}{a}, -\frac{\pi}{a}, \frac{\pi}{c})]$ and a, c are the lattice constants.

leads to a splitting of the peak structure in pDOS $\rho^d_m(\varepsilon_\mathrm{F})$ of the d_{xz} and d_{yz} orbitals [51]. In the nematic state as shown in Fig. 3, the E hexadecapoles become finite, which gives rise to the significant mixings among the $|\ell_z| = 2$ orbitals (d_{xy} and $d_{x^2-y^2}$) and $|\ell_z| = 1$ orbitals (d_{xz} and d_{yz}) [64]. The mixing with $d_{x^2-y^2}(d_{xy})$ having a large weight above (below) ε_F pushes down (up) the energy level of the mixed partner $d_{yz}(d_{xz})$. Such a mixing effect is remarkable in the M_y-Γ and A_y-Z directions as seen in Figs. 4(a) and 4(d): A mixing gap is formed near -0.1 eV in their directions. On the other hand, the band for the d_{xy} orbital near -0.2 eV in the M_x-Γ and A_x-Z directions remains almost unchanged. This one-side gap opening along the M_x-Γ-M_y direction, which is consistent with the experiment [36], is critically important for the origin of the nematic state because it inherently requires the presence of the E multipoles as pointed out in this Letter [65].

The orbital-dependent correlation effect due to Hund's coupling J, "Hund's metal" behavior, has been discussed in FeSe where the pressure- and correlation-driven Lifshitz transitions [66,67], and the enhancement of compressibility with a charge instability [68,69] have been obtained for the similar U values of the present nematic transition. Therefore, it will be important to extend the present method to a strongly correlated theory incorporating the properties of Hund's metal and to clarify the relation between the nematic states obtained here and Hund's metal phenomena [66–69], which is, however, beyond the scope of the present Letter.

To summarize, we have studied the nonmagnetic normal and nematic states of the iron-based superconductor FeSe by using the DFT+U method with the multipole analyses. The effect of U on the normal state generates a topological change in FSs from 3h-FSs to 2h-FSs, leading to a change in the dominant orbital near ε_F from d_{xy} to d_{xz}, d_{yz}. As a result, the multipolar nematic state with the E antiferrohexadecapoles accompanying the B_2 ferromultipoles has been obtained without any assumption of the order parameters, giving rise to both of the d_{xz}-d_{yz} orbital splitting at Γ and the d_{xy}-(d_{xz}, d_{yz}) orbital mixing around M and A points. From phenomenological analysis, we have found that the intermultipole coupling of B_2 and E multipoles on each Fe site can explain the energy gain larger for the coexisting order than for the quadupole O_{xy} order alone. This multipolar mechanism for the formation of nematic state will be applicable not only to FeSe, but also to other iron pnictides where the degenerated d_{xz}, d_{yz} orbitals play a crucial role.

This work was supported by the "Quantum Liquid Crystals" Grant No. JP19H05825 KAKENHI on Innovative Areas from JSPS of Japan.

[1] F.-C. Hsu, J.-Y. Luo, K.-W. Yeh, T.-K. Chen, T.-W. Huang, P. M. Wu, Y.-C. Lee, Y.-L. Huang, Y.-Y. Chu, D.-C. Yan, and M.-K. Wu, Proc. Natl. Acad. Sci. USA **105**, 14262 (2008).

[2] T. M. McQueen, A. J. Williams, P. W. Stephens, J. Tao, Y. Zhu, V. Ksenofontov, F. Casper, C. Felser, and R. J. Cava, Phys. Rev. Lett. **103**, 057002 (2009).

[3] Y. Mizuguchi and Y. Takano, J. Phys. Soc. Jpn. **79**, 102001 (2010).
[4] X. Liu, L. Zhao, S. He, J. He, D. Liu, D. Mou, B. Shen, Y. Hu, J. Huang, and X. J. Zhou, J. Phys.: Condens. Matter **27**, 183201 (2015).
[5] A. E. Böhmer and A. Kreisel, J. Phys.: Condens. Matter **30**, 023001 (2018).
[6] T. Shibauchi, T. Hanaguri, and Y. Matsuda, J. Phys. Soc. Jpn. **89**, 102002 (2020).
[7] A. Kreisel, P. J. Hirschfeld, and B. M. Andersen, Symmetry **12**, 1402 (2020).
[8] J. P. Sun, K. Matsuura, G. Z. Ye, Y. Mizukami, M. Shimozawa, K. Matsubayashi, M. Yamashita, T. Watashige, S. Kasahara, Y. Matsuda, J.-Q. Yan, B. C. Sales, Y. Uwatoko, J.-G. Cheng, and T. Shibauchi, Nat. Commun. **7**, 12146 (2016).
[9] T. Terashima, N. Kikugawa, S. Kasahara, T. Watashige, T. Shibauchi, Y. Matsuda, T. Wolf, A. E. Böhmer, F. Hardy, C. Meingast, H. v. Löhneysen, and S. Uji, J. Phys. Soc. Jpn. **84**, 063701 (2015).
[10] T. Terashima, N. Kikugawa, S. Kasahara, T. Watashige, Y. Matsuda, T. Shibauchi, and S. Uji, Phys. Rev. B **93**, 180503(R) (2016).
[11] S. Hosoi, K. Matsuura, K. Ishida, H. Wang, Y. Mizukami, T. Watashige, S. Kasahara, Y. Matsuda, and T. Shibauchi, Proc. Natl. Acad. Sci. USA **113**, 8139 (2016).
[12] A. I. Coldea, S. F. Blake, S. Kasahara, A. A. Haghighirad, M. D. Watson, W. Knafo, E. S. Choi, A. McCollam, P. Reiss, T. Yamashita, M. Bruma, S. C. Speller, Y. Matsuda, T. Wolf, T. Shibauchi, and A. J. Schofield, npj Quantm Mater. **4**, 2 (2019).
[13] A. E. Böhmer, F. Hardy, F. Eilers, D. Ernst, P. Adelmann, P. Schweiss, T. Wolf, and C. Meingast, Phys. Rev. B **87**, 180505(R) (2013).
[14] T. Shimojima, Y. Suzuki, T. Sonobe, A. Nakamura, J. O. M. Sakano, K. Yoshioka, M. Kuwata-Gonokami, K. Ono, H. Kumigashira, A. E. Böhmer, F. Hardy, T. Wolf, C. Meingast, H. v. Löhneysen, H. Ikeda, and K. Ishizaka, Phys. Rev. B **90**, 121111(R) (2014).
[15] A. E. Böhmer, T. Arai, F. Hardy, T. Hattori, T. Iye, T. Wolf, H. v. Löhneysen, K. Ishida, and C. Meingast, Phys. Rev. Lett. **114**, 027001 (2015).
[16] P. Massat, D. Farina, I. Paul, S. Karlsson, P. Strobel, P. Toulemonde, M.-A. Mĕasson, M. Cazayous, A. Sacuto, S. Kasahara, T. Shibauchi, Y. Matsuda, and Y. Gallais, Proc. Natl. Acad. Sci. USA **113**, 9177 (2016).
[17] W. Zhang, S. Wu, S. Kasahara, T. Shibauchi, Y. Matsuda, and G. Blumberg, Proc. Natl. Acad. Sci. USA **118**, e2020585118 (2020).
[18] M. Aichhorn, S. Biermann, T. Miyake, A. Georges, and M. Imada, Phys. Rev. B **82**, 064504 (2010).
[19] A. Liebsch and H. Ishida, Phys. Rev. B **82**, 155106 (2010).
[20] Z. P. Yin, K. Haule, and G. Kotliar, Nat. Mater. **10**, 932 (2011).
[21] N. Lanată, H. U. R. Strand, G. Giovannetti, B. Hellsing, L. de' Medici, and M. Capone, Phys. Rev. B **87**, 045122 (2013).
[22] S. Kasahara, T. Watashige, T. Hanaguri, Y. Kohsaka, T. Yamashita, Y. Shimoyama, Y. Mizukami, R. Endo, H. Ikeda, K. Aoyama, T. Terashima, S. Uji, T. Wolf, H. v. Löhneysen, T. Shibauchi, and Y. Matsuda, Proc. Natl. Acad. Sci. USA **111**, 16309 (2014).
[23] S. Kasahara, T. Yamashita, A. Shi, R. Kobayashi, Y. Shimoyama, T. Watashige, K. Ishida, T. Terashima, T. Wolf, F. Hardy, C. Meingast, H. v. Löhneysen, A. Levchenko, T. Shibauchi, and Y. Matsuda, Nat. Commun. **7**, 12843 (2016).
[24] T. Hanaguri, S. Kasahara, J. Böker, I. Eremin, T. Shibauchi, and Y. Matsuda, Phys. Rev. Lett. **122**, 077001 (2019).
[25] S. Kasahara, Y. Sato, S. Licciardello, M. Čulo, S. Arsenijević, T. Ottenbros, T. Tominaga, J. Böker, I. Eremin, T. Shibauchi, J. Wosnitza, N. E. Hussey, and Y. Matsuda, Phys. Rev. Lett. **124**, 107001 (2020).
[26] T. Terashima, N. Kikugawa, A. Kiswandhi, E.-S. Choi, J. S. Brooks, S. Kasahara, T. Watashige, H. Ikeda, T. Shibauchi, Y. Matsuda, T. Wolf, A. E. Böhmer, F. Hardy, C. Meingast, H. v. Löhneysen, M.-T. Suzuki, R. Arita, and S. Uji, Phys. Rev. B **90**, 144517 (2014).
[27] T. Terashima, N. Kikugawa, A. Kiswandhi, D. Graf, E.-S. Choi, J. S. Brooks, S. Kasahara, T. Watashige, Y. Matsuda, T. Shibauchi, T. Wolf, A. E. Böhmer, F. Hardy, C. Meingast, H. v. Löhneysen, and S. Uji, Phys. Rev. B **93**, 094505 (2016).
[28] K. Nakayama, Y. Miyata, G. N. Phan, T. Sato, Y. Tanabe, T. Urata, K. Tanigaki, and T. Takahashi, Phys. Rev. Lett. **113**, 237001 (2014).
[29] J. Maletz, V. B. Zabolotnyy, D. V. Evtushinsky, S. Thirupathaiah, A. U. B. Wolter, L. Harnagea, A. N. Yaresko, A. N. Vasiliev, D. A. Chareev, A. E. Böhmer, F. Hardy, T. Wolf, C. Meingast, E. D. L. Rienks, B. Büchner, and S. V. Borisenko, Phys. Rev. B **89**, 220506(R) (2014).
[30] M. D. Watson, T. K. Kim, A. A. Haghighirad, N. R. Davies, A. McCollam, A. Narayanan, S. F. Blake, Y. L. Chen, S. Ghannadzadeh, A. J. Schofield, M. Hoesch, C. Meingast, T. Wolf, and A. I. Coldea, Phys. Rev. B **91**, 155106 (2015).
[31] Y. Suzuki, T. Shimojima, T. Sonobe, A. Nakamura, M. Sakano, H. Tsuji, J. Omachi, K. Yoshioka, M. Kuwata-Gonokami, T. Watashige, R. Kobayashi, S. Kasahara, T. Shibauchi, Y. Matsuda, Y. Yamakawa, H. Kontani, and K. Ishizaka, Phys. Rev. B **92**, 205117 (2015).
[32] P. Zhang, T. Qian, P. Richard, X. P. Wang, H. Miao, B. Q. Lv, B. B. Fu, T. Wolf, C. Meingast, X. X. Wu, Z. Q. Wang, J. P. Hu, and H. Ding, Phys. Rev. B **91**, 214503 (2015).
[33] M. D. Watson, T. K. Kim, L. C. Rhodes, M. Eschrig, M. Hoesch, A. A. Haghighirad, and A. I. Coldea, Phys. Rev. B **94**, 201107(R) (2016).
[34] M. D. Watson, A. A. Haghighirad, L. C. Rhodes, M. Hoesch, and T. K. Kim, New J. Phys. **19**, 103021 (2017).
[35] H. Pfau, S. D. Chen, M. Yi, M. Hashimoto, C. R. Rotundu, J. C. Palmstrom, T. Chen, P.-C. Dai, J. Straquadine, A. Hristov, R. J. Birgeneau, I. R. Fisher, D. Lu, and Z.-X. Shen, Phys. Rev. Lett. **123**, 066402 (2019).
[36] M. Yi, H. Pfau, Y. Zhang, Y. He, H. Wu, T. Chen, Z. R. Ye, M. Hashimoto, R. Yu, Q. Si, D.-H. Lee, P. Dai, Z.-X. Shen, D. H. Lu, and R. J. Birgeneau, Phys. Rev. X **9**, 041049 (2019).
[37] A. Subedi, L. Zhang, D. J. Singh, and M. H. Du, Phys. Rev. B **78**, 134514 (2008).
[38] H. Lohani, P. Mishra, and B. Sekhar, Physica C **512**, 54 (2015).
[39] S. Mandal, R. E. Cohen, and K. Haule, Phys. Rev. B **89**, 220502(R) (2014).
[40] J. M. Tomczak, M. van Schilfgaarde, and G. Kotliar, Phys. Rev. Lett. **109**, 237010 (2012).

[41] Y. Yamakawa, S. Onari, and H. Kontani, Phys. Rev. X **6**, 021032 (2016).
[42] Y. Yamakawa and H. Kontani, Phys. Rev. B **96**, 144509 (2017).
[43] J. Ishizuka, T. Yamada, Y. Yanagi, and Y. Ono, J. Phys. Soc. Jpn. **87**, 014705 (2018).
[44] Y. Su, H. Lian, and T. Li, J. Phys.: Condens. Matter **27**, 105702 (2015).
[45] S. Onari, Y. Yamakawa, and H. Kontani, Phys. Rev. Lett. **116**, 227001 (2016).
[46] R.-Q. Xing, L. Classen, and A. V. Chubukov, Phys. Rev. B **98**, 041108(R) (2018).
[47] J. Kang, R. M. Fernandes, and A. Chubukov, Phys. Rev. Lett. **120**, 267001 (2018).
[48] X. Long, S. Zhang, F. Wang, and Z. Liu, npj Quantum Mater. **5**, 50 (2020).
[49] D. Steffensen, A. Kreisel, P. J. Hirschfeld, and B. M. Andersen, Phys. Rev. B **103**, 054505 (2021).
[50] L. C. Rhodes, J. Böker, M. A. Müller, M. Eschrig, and I. M. Eremin, npj Quantum Mater. **6**, 45 (2021).
[51] See Supplemental Material at http://link.aps.org/supplemental/10.1103/PhysRevB.104.L161110 for which is includes Refs. [70–72].
[52] P. Blaha, K. Schwarz, F. Tran, R. Laskowski, G. K. H. Madsen, and L. D. Marks, J. Chem. Phys. **152**, 074101 (2020).
[53] A. B. Shick, A. I. Liechtenstein, and W. E. Pickett, Phys. Rev. B **60**, 10763 (1999).
[54] F. Tran, J. Kuneš, P. Novák, P. Blaha, L. D. Marks, and K. Schwarz, Comput. Phys. Commun. **179**, 784 (2008).
[55] Here we also check $\varepsilon_{\boldsymbol{k}n} - \varepsilon_{\rm F}$ around $\varepsilon_{\rm F}$ for the hole (electron) bands at Γ and Z (M and A) points as a function U, and we obtain a continuous tracking of the connection from the 3h-FSs and 2h-FSs together with a critical interaction of the Lifshitz transition $U_{\rm LT}$, which is one of the new results for the present Letter in contrast to the previous DFT $+U$ study [38] where the 2h-FSs were obtained only for several large values of U.
[56] Throughout the calculation, total d occupation number $n^{d,\nu}$ is almost unchanged from $n^{d,\nu} = 6.17$–6.19, and the total valence electron number $n_{\rm v}$ is strictly fixed $n_{\rm v} = 60$ per two (FeSe) in the unit cell where 28 electrons are attributed to Fe-3p, 3d, 4s and 32 electrons to Se-3d, 4s, 4p.
[57] M. Weinert, E. Wimmer, and A. J. Freeman, Phys. Rev. B **26**, 4571 (1982).
[58] H. Kusunose, J. Phys. Soc. Jpn. **77**, 064701 (2008).
[59] S. Hayami, M. Yatsushiro, Y. Yanagi, and H. Kusunose, Phys. Rev. B **98**, 165110 (2018).
[60] M.-T. Suzuki, N. Magnani, and P. M. Oppeneer, Phys. Rev. B **88**, 195146 (2013).
[61] M.-T. Suzuki, H. Ikeda, and P. M. Oppeneer, J. Phys. Soc. Jpn. **87**, 041008 (2018).
[62] H. Kusunose and Y. Kuramoto, J. Phys. Soc. Jpn. **70**, 1751 (2001).
[63] Here we normalize the multipoles as $\frac{1}{d}{\rm Tr}[X_\alpha X_\beta] = \delta_{\alpha\beta}$ with $d = 5$ unlike the calculation of the density matrix $n^{\nu}_{mm'}$.
[64] Here we note that the E quadrupoles O_{zx}, O_{yz} also induce the similar mixings, but their hybridizations are partial and incomplete since in $|m\rangle$ orbital basis with $m = -2, \dots, +2$, O_{Γ_γ} with Γ_γ=zx, yz has only finite elements as $\langle m|O_{\Gamma_\gamma}|m \pm 1\rangle$, whereas the hexadecapoles $Q_{4\Gamma_\gamma}$ with Γ_γ=α, $x(y)$ and β, $x(y)$ have finite elements as $\langle m|Q_{4\Gamma_\gamma}|m \pm 3\rangle$ in addition to $\langle m|Q_{4\Gamma_\gamma}|m \pm 1\rangle$.
[65] On the other hand, the sign-reversing nematic splitting observed in experiments cannot be reproduced by the present DFT+U method that is a kind of local approximation since it requires the effect of wave-vector-dependent (nonlocal) self-energy corrections beyond the mean-field approximation of the local interaction under a model whose parameters are adjusted to reproduce the FSs of the ARPES experiment as in Ref. [45]. Such nonlocal effects could be described by incorporating, for example, the mean-field approximation for the intersite Coulomb interactions, inducing additional hopping terms into our method.
[66] S. L. Skornyakov, V. I. Anisimov, D. Vollhardt, and I. Leonov, Phys. Rev. B **97**, 115165 (2018).
[67] S. L. Skornyakov and I. Leonov, Phys. Rev. B **100**, 235123 (2019).
[68] P. V. Arribi and L. de' Medici, Phys. Rev. Lett. **121**, 197001 (2018).
[69] M. Chatzieleftheriou, M. Berović, P. V. Arribi, M. Capone, and L. de' Medici, Phys. Rev. B **102**, 205127 (2020).
[70] J. P. Perdew, K. Burke, and M. Ernzerhof, Phys. Rev. Lett. **77**, 3865 (1996).
[71] V. I. Anisimov, I. V. Solovyev, M. A. Korotin, M. T. Czyżyk, and G. A. Sawatzky, Phys. Rev. B **48**, 16929 (1993).
[72] J. K. Glasbrenner, I. I. Mazin, H. O. Jeschke, P. J. Hirschfeld, R. M. Fernandes, and R. Valentí, Nat. Phys. **11**, 953 (2015).